NASA

Technical Memorandum 86167

SIMULTANEOUS OCEAN CROSS-SECTION AND RAINFALL MEASUREMENTS FROM SPACE WITH A NADIR-POINTING RADAR

Robert Meneghini and David Atlas

NOVEMBER 1984

National Aeronautics and
Space Administration

Goddard Space Flight Center
Greenbelt, Maryland 20771

TM-86167

SIMULTANEOUS OCEAN CROSS-SECTION AND RAINFALL MEASUREMENTS FROM SPACE WITH A NADIR-POINTING RADAR

Robert Meneghini and David Atlas

November 1984

GODDARD SPACE FLIGHT CENTER
Greenbelt, Maryland 20770

ABSTRACT

In the case of a nadir-looking space-borne or aircraft radar in the presence of rain the return power corresponding to secondary surface reflections may provide information on the scattering properties of the surface and the precipitation. The object of the present study is to evaluate a method for determining simultaneously the rainfall rate and the normalized backscattering cross section of the surface, σ°. The method is based upon the mirror-reflected power, P_m, which corresponds to the portion of the incident power scattered from the surface to the precipitation, intercepted by the precipitation, and again returned to the surface where it is scattered a final time back to the antenna. Two approximations are obtained for P_m depending on whether the field of view at the surface is either much greater or much less than the height of the reflection layer. Since the dependence of P_m on the backscattering cross section of the surface differs in the two cases, two algorithms are given by which the path-averaged rain rate and σ° can be deduced. We also discuss the detectability of P_m, the relative strength of other contributions to the return power arriving simultaneous with P_m, and the validity of the approximations used in deriving P_m.

SIMULTANEOUS OCEAN CROSS-SECTION AND RAINFALL MEASUREMENTS FROM SPACE WITH A NADIR-POINTING RADAR

1. INTRODUCTION

The importance of measuring precipitation globally has been discussed on many occasions (e.g., Atlas and Thiele, 1981). In the latter work, a broad spectrum of experts reviewed the state of the art and prospects for making precipitation measurements from space. Subsequently, Atlas et al. (1982) assessed a variety of spaceborne radar methods. This paper is a variation upon one of the methods discussed there, namely the surface reference method or SRT. The latter technique is treated in greater detail by Meneghini et al. (1983). One of its major shortcomings was the need to estimate the normalized backscattering cross section of the surface, σ°, independently in order that the rainfall rate could be measured.

We shall show that for a nadir-looking radar, the present method offers the potential of measuring both the ocean radar cross-section σ° and the path average rain rate simultaneously. This represents an improvement over the SRT method in that σ° can be obtained directly from the measured powers.

This paper is a revision of an earlier, preliminary study on the same subject (Atlas and Meneghini, 1983). Here we derive expressions for the mirror-reflected power under fewer restrictions and discuss the error sources in more detail. Nevertheless, a rigorous error analysis is beyond the scope of this paper. Therefore, the study should be viewed as a first step in addressing the questions of the nature of the secondary surface reflections and in determining whether meteorological information can be extracted from such data.

2. BASIC CONCEPT

The basic concept of the method is an extension of the approach proposed by Eckerman et al., (1978). In essence, they proposed measurements of the surface radar cross-section in the absence of rain from either measurements outside of the rain in the immediate vicinity, or

from a look-up table generated from prior observations. The path average rain rate would then be deduced from the microwave attenuation calculated as a difference between the echo expected in the absence of rain and that actually measured, and using well established relations between attenuation and rain rate. Dual wavelength versions of this method also have been described (Moore, 1981; Atlas et al., 1982).

The primary limitation of the method focused around the accuracy with which one could expect to estimate the surface radar cross-section. Indeed, the minimum detectable rain rate was found to be dependent upon the RMS error of this estimate.

It is noteworthy that Inomata et al. (1981) conducted an aircraft experiment with two radars operating at 0.86 and 3.2 cm. By simply taking the ocean surface cross-section, 10 log σ°, at nadir to be a constant 10 db at 0.86 cm, they were able to compute the attenuation at this wavelength and the average rain rate between the surface and the melting level. These values correlated well with those computed from measurements of the 3.2 cm reflectivity factor, Z, and resulted in a Z-R relationship close to those generally accepted (Battan, 1973). More recently, Fujita et al. (1984) have found fair to good correlations between path-averaged attenuation as estimated from the surface reference method and a dual-wavelength algorithm (Fujita, 1983). They note that the major source of error is probably caused by the variability in σ°. Indeed the nadir ocean surface cross-section is sensitive to roughness and thus decreases with windspeed (Moore and Fung, 1979). This sensitivity has been exploited in estimating ocean surface wind speeds from space (Fedor and Brown, 1982).

To reduce the errors caused by the variability in σ° at least two approaches are possible. The first is to introduce a second radar wavelength and make use of the fact that the σ° at the two wavelengths are well correlated, thus allowing measurements of differential path attenuation. A second approach is to attempt to measure both σ° and rainfall attenuation simultaneously at a single wavelength. This paper is concerned exclusively with the latter approach for

the special case of a nadir-looking radar over the sea. Although the method is applicable to sensing over the land as well, higher transmit powers are needed to obtain detectable signal levels.

The scattering geometry is illustrated schematically in Fig. 1. Fig. 1a shows a nadir pointing radar beam viewing the ocean through a storm. In the absence of rain, the echo power is a measure of the ocean backscatter cross section per unit area σ°. With a rainstorm in the path, the power is attenuated by A db, which is a measure of the path average rain rate, $\bar{R}$, (Atlas and Ulbrich, 1977). The latter authors show that, in the absence of vertical air motions, A(dB) is essentially linear with R regardless of the drop size distribution at 0.9 cm and approximately so in the band from about 0.7 to 2 cm. To get a true measure of A and thus of R (assuming the attenuating path length is known) it is necessary to know σ°.

Figure 1b illustrates the path of a ray from the radar through the precipitation, scattered from the ocean surface back to a slab of precipitation at height H, scattered back to the ocean, and finally reflected once more from the ocean surface and passing through the precipitation back to the radar receiver. The paths of the radar transmitter and receiver are displaced from one another for ease of displaying the incoming and outgoing rays. Of course similar mirror reflected echoes of the precipitation are received from all heights from which they are detectable.

Figure 1c shows a schematic of the radar return power as a function of range, or equivalently, time. The first contribution received is the direct backscatter from the precipitation, P_d, followed by the echo from the surface at height zero, P_g. At still later times the sum of all scattering mechanisms corresponding to ray paths greater than $2H_o$ (where H_o is the satellite altitude) will arrive at the receiver. As indicated in the figure, one set of ray paths corresponds to the mirror-reflected backscatter, P_m. In addition, other multi-path contributions will be present as well as the return from the surface received along the antenna side-lobes. If the mirror-reflection component dominates, then it can be seen that a single series of measurements made along the range direction will yield P_d, P_g and P_m. In the next section we show

that under certain conditions the three unknown quantitites, σ°, the rain attenuation and rain reflectivity can be found from the above measurables.

3. DERIVATION

To simplify the equations, we introduce the quantities A_j, $j = 1, \ldots, n$

$$A_j = \int_0^{H_j} k\,(s)\,ds \tag{1}$$

where H_j is the height of the jth range gate as measured from the surface. Letting the storm height H_s correspond to the n^{th} range gate, i.e., $H_s = H_n$, then A_n represents the one way attenuation through the precipitation.

With this notation, the average echo power from the ocean surface under beam-limited conditions can be written (Appendix II)

$$P_g = (C_g\,\sigma^\circ/H_o^2)\;\; 10^{-0.2\,A_n} \tag{2}$$

where the symbols are defined in Appendix I, and the constant C_g is approximately

$$C_g = 7 \times 10^{-3}\,\lambda^2\,P_T/\theta_b^2 \tag{3}$$

Similarly, the echo power received directly from the precipitation at height H_j above the surface corresponding to a time of arrival of t_j prior to that of the ground echo, is given by

$$P_d(-t_j) = C_d\,\eta_j/(H_o - H_j)^2\;\; 10^{-0.2\,(A_n - A_j)} \tag{4}$$

where

$$C_d = 3.5 \times 10^{-3}\,\lambda^2\,P_T\,L/\theta_b^2 \tag{5}$$

and where η_j is the rain reflectivity in the jth range gate above the surface.

Under several simplifying assumptions, the expression for the mirror reflected power, measured at a time t_j subsequent to that of the ground return can be written as (Appendix II)

$$P_m(t_j) = 3.5 \times 10^{-3} \frac{\lambda^2 P_T \eta_j \Gamma^4 L \sigma^\circ 10^{-0.2 (A_n + A_j)}}{\sigma^\circ \rho_o^2 + 2.76 \Gamma^2 H_j^2} \quad (6)$$

where ρ_o is the radius of the field of view (FOV) given by

$$\rho_o = \theta_b H_o \quad (7)$$

For notational convenience we let $q = (\sigma^\circ/2.76 \Gamma^2)^{1/2}$. Thus, when the height of the reflection layer, H_j, is either much greater or much less than $q\rho_o$, the mirror-reflected return power can be approximated by one of the following expressions

$$P_m(t_j) = \begin{cases} \dfrac{C_m' \eta_j \sigma^\circ \Gamma^2}{H_j^2} 10^{-0.2 (A_n + A_j)} ; H_j >> q\rho_o & (8) \\ \dfrac{C_m \eta_j \Gamma^4}{H_o^2} 10^{-0.2 (A_n + A_j)} : H_j << q\rho_o & (9) \end{cases}$$

where Γ^2 is the Fresnel reflectivity of the surface and

$$C_m' = 1.26 \times 10^{-3} \lambda^2 P_T L \quad (10)$$

$$C_m = C_d = 3.5 \times 10^{-3} \lambda^2 P_T L / \theta_b^2 \quad (11)$$

The approximation to P_m given by (8), apart from a constant factor that depends only on the particular antenna pattern function assumed, is the same as previously derived (Atlas and Meneghini, 1983). On the other hand, when $H_j << q\rho_o$ and $H_o >> H_j$, P_m is the same as would be derived for the mirror reflected power from a perfectly smooth surface. In fact, in this latter case, a ratio of (9) to (4) yields Γ^4 10**(-0.4 A) which implies that the ratio of the mirror-reflected power to the direct power near the surface, where $A_j \approx 0$, is approximately equal to the square of the Fresnel reflectivity of the surface.

There are several features of equations (8) and (9) that are of interest: (1) the precipitation parameters (reflectivity and attenuation) enter in the same way in both approximations;

(2) For $H_j >> q\rho_o$, P_m is independent of the antenna parameters and satellite altitude but dependent on the height of the reflection layer, H_j, while for $H_j << q\rho_o$, P_m is inversely proportional to the area of the FOV but independent of H_j; (3) for $H_j >> q\rho_o$, P_m is directly proportional to σ° while for $H_j << q\rho_o$, P_m is independent of σ°.

Before discussing equations (8) and (9) it is worthwhile first to comment on why the form of P_m should change according to whether $H_j >> q\rho_o$ or $H_j << q\rho_o$. Consider a small volume element containing precipitation located along the vertical at a height H_j above the surface and upon which is incident a ray scattered from the surface. If $2\rho_o >> H_j$ then the majority of the energy scattered from the precipitation volume will be returned to the illuminated portion of the surface. However, if $H_j >> 2\rho_o$, then of the energy scattered from the precipitation volume, only those rays nearly anti-parallel to the incident ray will be returned to the illuminated portion of the surface. In the former case, the precipitation is analogous to a mirror with a 'reflection coefficient' of η_j; in other words, apart from the energy transmitted through the precipitation, all the energy incident on the precipitation is returned to the illuminated portion of the surface. On the basis of this difference we can expect the form of P_m to change according to whether H_j is much greater of much less than the diameter of the FOV, i.e., $2\rho_o$. Of course, this argument does not account for the fact that the actual quantity to be compared to H_j is not $2\rho_o$ but $q\rho_o$ and therefore is a function of σ° and Γ^2 as well as ρ_o.

An understanding of the dependence of P_m on σ° may be gained by considering radiation incident on a surface area element which is scattered bistatically out to the precipitation, a portion of which is returned to a second surface element. The final process is the scattering from the secondary area element back to the antenna. The total mirror reflected power, therefore, is given by the double sum of all such primary and secondary scattering elements within the illuminated surface region.

In the notation of Appendix II the total mirror-reflected power is proportional to J where

$$J = \int_{\underline{x}_1} \int_{\underline{x}_2} I(\underline{x}_1, \underline{x}_2)\, e^{-\beta^2 (|x_1|^2 + |x_2|^2)}\, d\underline{x}_1\, d\underline{x}_2 \qquad (12)$$

and where $\underline{x}_1$, $\underline{x}_2$, are the locations of the primary and secondary surface scattering elements. The exponential term of the integrand represents the antenna pattern function at $\underline{x}_1$ and $\underline{x}_2$, with $\beta = \gamma^2/\rho_0{}^2$, $\gamma = 0.86$. It may be shown numerically that a good approximation to $I(\underline{x}_1, \underline{x}_2)$ is

$$I(\underline{x}_1, \underline{x}_2) = I_s\, e^{-\alpha^2 |\underline{x}_1 - \underline{x}_2|^2} \qquad (13)$$

where, for $\sigma^\circ >> \Gamma^2$, $H_j >> L$

$$I_s = \pi L \Gamma^2 \sigma^\circ / H_j{}^2 \qquad (14)$$

$$\alpha^{-2} = a_e{}^2 = 8\Gamma^2 H_j{}^2 / \sigma^\circ \qquad (15)$$

A heuristic argument for the form of $I(\underline{x}_1, \underline{x}_2)$ given by (13) is presented in Appendix II. In this approximation, $I(\underline{x}_1, \underline{x}_2)$ is a function only of the separation between the scattering centers. As the separation distance goes to zero, $I(\underline{x}_1, \underline{x}_2)$ reduces to I_s which is directly proportional to σ°. On the other hand, the distance between the scattering centers for which

$$I(\underline{x}_1, \underline{x}_2) = I_s\, e^{-1}$$

is equal to a_e which in turn is inversely proportional to $\sqrt{\sigma^\circ}$. We can interpret this last result in the following way: about each primary scattering element on the surface, $\underline{x}_1$, there corresponds a secondary scattering region of dimension a_e, centered at $\underline{x}_1$, which contributes the majority of the power returned to the antenna. This last statement must be qualified, however, if $a_e >> \rho_0$ since in this case ρ_0, the radius of the FOV, determines the effective

dimension of the secondary scattering region. In other words, the secondary scattering area can be defined approximately by

$$A_e = \min(\pi a_e^2, \pi\rho_o^2)$$

To understand this in a more quantitative manner we assume for simplicity that $\underline{x}_1$, centered at the surface area element ΔA_1, is located at the center of the FOV, i.e. $|\underline{x}_1| = \rho_1 = 0$. The contribution to the mirror reflected power is then

$$J_1 = 2\pi \Delta A_1 \int_0^\infty I_s e^{-\rho^2(\alpha^2 + \beta^2)} \rho \, d\rho$$

or

$$J_1 = \frac{\pi \Delta A_1 I_s \rho_o^2 a_e^2}{\rho_o^2 + \gamma^2 a_e^2}$$

Thus

$$J_1 = \pi \Delta A_1 I_s \begin{cases} \rho_o^2/\gamma^2 & ; \ \gamma a_e >> \rho_o \\ a_e^2 & ; \ \gamma a_e << \rho_o \end{cases}$$

Since I_s and a_e^{-2} are directly proportional to σ°, the above equations show that J_1 is independent of σ° for $\gamma a_e << \rho_o$ while J_1 is directly proportional to σ° for $\gamma a_e >> \rho_o$. This accounts for the σ° dependence in equations (8) and (9). The dependencies of P_{in} on the antenna parameters and satellite and reflection layer altitudes can be found by summing the contributions from all primary surface scattering elements (Appendix II).

4. ALGORITHMS

Case I: $H_j >> q\rho_o$; Height of reflection layer much larger than diameter of FOV

To obtain an algorithm that yields path attenuation and thus mean rainfall rate, we note that equations (4) and (8) are functions of η_j thus allowing its elimination. Explicitly,

$$\frac{P_m(t_j)}{P_d(-t_j)} = \frac{C_m' \, \sigma^\circ \, \Gamma^2 \, (H_o - H_j)^2}{C_d \, H_j^2} \; 10^{-0.4 A_j} \tag{16}$$

To eliminate σ°, (2) is used in (16). Taking the logarithm of the result yields

$$2A_j - A_n = 5 \left\{ - \text{Log} \, [P_m(t_j)/P_d(-t_j) \, P_g] + S_j + S_o \right\} \tag{17}$$

where

$$S_j = \text{Log} \, [H_o^2 \, (H_o^2 - H_j^2) \, \Gamma^2/H_j^2] \tag{18}$$

$$S_o = \text{Log} \, (C_m'/C_d \, C_g) \tag{19}$$

When the range gate at the storm top is chosen, $H_n = H_s$, (17) reduces to an estimate for the total one-way attentuation, A_n:

$$A_n = 5 \left\{ - \text{Log} \, [P_m(t_n)/P_d(-t_n) \, P_g] + S_n + S_o \right\} \tag{20}$$

From (20), a measurement of H_s, and the k-R relationship, the path-averaged rain rate can be deduced (Atlas and Ulbrich; 1977).

The estimate of attenuation given by (20) depends upon the calibration constants C_m', C_d, C_g through the term S_o. If we assume that detectable levels of P_m can be obtained in light rain (where the attenuation is negligible), then the left hand side of (20) is approximately zero. This implies that a best-fit value of S_o can be obtained from measurements of P_m and P_d near the storm top under conditions of light rain. Returning to (20) and comparing it with (2) shows that σ° can be found from the equation

$$\sigma^\circ = (P_g \, H_o^2/C_g) \; 10^{0.2 A_n} \tag{21}$$

The vertical profiles of reflectivity factors, η_j, and the associated rain rates R_j can be ob-

tained from A_n, equation (20), and measurements of $P_d(-t_j)$ via the Hitschfeld-Bordan algorithm (see Lu and Hai, 1980; Meneghini et al., 1983).

Case II: $H_j \ll q\rho_o$; Height of reflection layer much less than diameter of FOV

As in the first case, we begin by taking the ratio of P_m to P_d where P_m is now given by (9):

$$\frac{P_m(t_j)}{P_d(-t_j)} = \frac{C_m \Gamma^4 (H_o - H_j)^2}{C_d H_o^2} \cdot 10^{-0.4 A_j} \qquad (22)$$

Noting that $C_m = C_d$, then

$$A_j = \frac{5}{2} \left\{ \text{Log} \left(\frac{P_m(t_j)}{P_d(-t_j)} \right) + 2 \text{ Log} \left(\frac{H_o}{\Gamma^2 (H_o - H_j)} \right) \right\} \qquad (23)$$

Setting j = n in (23) again provides an estimate for the total path integrated attenuation, A_n. Estimates of σ° and the range-profiled rain rates are found by a procedure identical to that previously described. It is not necessary to assume that C_m and C_d are equal, however. Since these quantities are range independent, it is clear from (22) that the interval attenuation between range gates k and j can be found. Solving for A_{jk} where $A_{jk} = \int_{r_k}^{r_j} k(s)\, ds$, $r_j > r_k$ we obtain

$$A_{jk} = -\frac{5}{2} \left\{ \text{Log} \left[\frac{P_m(t_j) P_d(-t_k)}{P_m(t_k) P_d(-t_j)} \right] + 2 \text{ Log} \left(\frac{H_o - H_k}{H_o - H_j} \right) \right\} \qquad (24)$$

For $H_o \gg H_n$, the second term is negligible and equation (24) is essentially the same as would be obtained for a dual-wavelength algorithm (Eccles and Mueller, 1971) if we interpret P_m and P_d respectively as the attenuating and nonattenuating wavelength returns from the jth and kth range gates. In the dual-wavelength algorithm, the reflectivity factors are assumed to be equal at each range gate, i.e., independent of wavelength. The analogous assumption here is that the reflectivity of the directly viewed rain volume is identical to that of the rain volume viewed via the first reflection from the surface (see section 6.3).

5. PRELIMINARY RESULTS

The first objective is to determine how the mirror reflected precipitation echo behaves with respect to that directly scattered and that received from the surface. We also want to know the dynamic range of rain rates over which we can expect detectable mirror echoes, the smallest of the three measureables. For the purpose of these calculations we have assumed the radar, storm, and ocean parameters shown in Table 1. Initially we assume a very large antenna diameter of 7.5 m to ensure that $H_s \gg q\rho_o$ and therefore that equation (8) is applicable. The effects of reducing the antenna size on P_m are discussed below.

Table 1: Model Radar, Storm, and Ocean Parameters

Parameter	Value
Wavelength – λ	1.87 cm
Peak Power – P_T	10 kw
Pulse Width – τ	1.33 sec
Antenna Diameter – D	7.5 m
Radar Noise Figure	7.0 dB
Orbit Height – H_o	500 km
Top of rain – H_s	3 km
Ocean Cross-Section – σ^o	10 dB
Range Resolution – L/2	0.2 km

We also use $\sigma^o = 10$ which corresponds to a wind speed of about 10 ms^{-1}. Table 2 shows values of 10 Log σ^o versus wind speed for the SEASAT 13.5 GHz radar (Fedor and Brown, 1982)

Table 2: Ocean Normalized Backscatter Cross-Sections (10 Log σ^o) at Nadir Versus Windspeed (Fedor and Brown, 1982)

Windspeed (ms^{-1})	1	3	5	10	20	50	100
Cross-Section (dB)	19.5	13.5	11.8	9.7	7.2	5.1	4.0

The results are shown in Fig. 2. All curves are signal to noise versus rain rate on a single pulse basis. To use a uniform scale for all three quantities the plotted values of 10 Log(P_g/N),

corresponding to the sea echo, have been reduced by 60 dB while the values of the direct rain return to noise. 10 Log(P_d/N) have been reduced by 11 dB. Clearly, with such a powerful radar there is an abundance of surface signal with the signal to noise curve remaining approximately constant at about 73 dB up to moderate rain rates beyond which the two-way attenuation through the 3 km depth of rain increases sharply.

The curve of 10 Log(P_d/N), corresponding to the echo received directly from the precipitation in the range gate immediately above the surface, exhibits adequate dynamic range with values exceeding 7 db over the full range from 0.1 to 100 mm/hr. At R < 10 mm/hr, 10 Log P_d is proportional to 15.2 Log R corresponding to the assumed Z - R relation, Z = 424 $R^{1.52}$. At R > 40 mm/hr, the curve is dominated by attenuation and the slope is proportional to ~ 22 Log R corresponding to a two way path through rain with an attenuation coefficient k = 0.042 $R^{1.1}$ db/km. That is to say that a 10-fold increase in R produces a 22 db increase in attenuation and corresponding decrease in received power.

For present purposes the most interesting curve is 10 Log (P_m/N) corresponding to the range gate at the top of the rainfall at 3 km height. At low rain rates where attenuation is negligible P_d is approximately 11 dB greater than P_m and the curves are parallel to one another. As the rain rate increases, the behavior of the ratio P_m/P_d is dominated by the attenuation term for a two way path between the surface and height H_j. For the case shown, the gate for the mirror-reflected power is positioned at the top of the rain area, H_j = 3 km, so that the attenuation terms for P_g and P_d are half that for P_m. When the range gates of the mirror reflection and the direct precipitation returns are near the ocean surface, the attenuation terms in P_m, P_d and P_g are approximately equal.

As mentioned earlier, the size of the antenna was chosen to insure the validity of equation (8); i.e., using the approximations $\rho_o = \theta_b H_o$, $\theta_b = \lambda/2D$ and D = 7.5 m yield ρ_o = 0.62 km which is much less than the maximum height of the reflection layer. For D = 1 m, $H_s \ll \rho_o$ so that P_m is given by equation (9). As shown in Fig. 3, P_m/N is reduced by about 7 dB from

the previous case and the range of rain rates for which P_m/N exceeds unity is between about 1.0 mm hr^{-1} and 30 mm hr^{-1}. It is also worth noting that at light rains (before the effects of attenuation are evident) P_d exceeds P_m by about 4.4 db. This difference, which is present as long as $H_j \ll q\rho_0$ results entirely from the fact that a ratio of equation (9) to equation (4) is equal to Γ^4 10**(- $0.4A_j$), which for light rain rates and $\Gamma^2 = 0.6$, is equal to - 4.4 dB.

In Table 3 we present the range of rain rates for which P_m/N exceeds unity for selected values of antenna diameter and radar wavelength, for values of the peak transmit power of 1 kw and 10 kw. We see that the 1 kw system is inadequate with a 1 m diameter antenna. At 3.2 cm, a combination of 1 kw and 3 m antenna diameter would serve well except at the light rain rates. On the other hand, with 10 kw, a 1 m antenna diameter provides adequate signal to noise over the lighter rain rates up to about 8 mm/hr at 0.86 cm, but quickly looses signal at the larger rain rates where attenuation is excessive. Thus, in order to achieve sufficient dynamic range in rain rate, we require a dual wavelength system. This is the case for any method, radar or radiometric, which relies on rainfall attenuation (Atlas et al., 1984). We should note, nevertheless, that the condition required for the present method, $P_m \gg N$, is significantly more stringent than the condition $P_g \gg N$, needed in the surface reference methods.

Table 3: Range of Rain Rates (mm hr^{-1}) for which P_m/N exceeds unity. The results in brackets correspond to P_T = 1 kw; otherwise P_T = 10 kw.

		Wavelength (cm)		
		0.86	1.87	3.2
Antenna Diameter (m)	1	0.1 mm hr^{-1} → 8 mm hr^{-1} [1.25 mm hr^{-1} → 3.2 mm hr^{-1}]	1 → 30 [none]	4 → 70 [none]
	3	0.1 → 10 [0.25 → 5]	0.3 → 40 [1.5 → 2.5]	1.3 → 100 [6.0 → 64]
	7.5	0.1 → 10 [0.25 → 6.5]	0.2 → 40 [1 → 25]	0.5 → 100 [2.5 → 80]

6. SOURCES OF ERROR

There are a number of difficulties associated with the method that must be resolved before establishing its feasibility. Some of the difficulties are common to all meteorological radar methods; e.g., sampling errors and errors caused by fluctuations in the drop size distribution. Other errors are, for the most part, characteristic of the method itself. Unfortunately, a rigorous error analysis requires a knowledge of the bistatic cross sections of the rain drops, a specification of the antenna pattern and the evaluation of a seven-fold integral. In the following sections, we discuss in a qualitative manner the error sources and indicate the circumstances under which they may be significant.

6.1 Multi-path and side-lobe contributions

There are a number of other scattering mechanisms that correspond to ray paths whose distances are equal to the mirror reflected path. Since these contributions arrive at the receiver at the same time as P_m, they constitute a source of error. Two kinds of paths are the dominant contributors to this error. The first is the direct backscattered power from the surface along the antenna side lobes.

To find the direct side lobe contribution that arrives at the receiver simultaneously with P_m, we set the path length of the mirror reflection equal to the path length of the side lobe contribution. This condition along with a knowledge of D/λ and the antenna pattern function specify the side lobe(s) of interest. As an example, we assume that the primary reflector has a parabolic illumination function which produces an electric field in the far zone of the form (Silver, 1949)

$$E = 8 J_2(x)/x^2$$

where $x = \pi D \sin\theta/\lambda$ and J_2 is the Bessel function of the first kind of second order. For a mirror-reflection height of 3 km and for the parameters of Table 1, the side lobe that arrives at the same time as P_m is well beyond the 10th side lobe and therefore negligible in compar-

ison to P_m. If the antenna diameter is decreased to 1 m, the nearest side lobe of interest is the fifth. To obtain an upper bound on this contribution we take the maximum value of the gain within the fifth side lobe and the region of scattering to be equal to the area of the annulus $\pi H_o L$. This procedure gives a side-lobe to noise ratio, P_{SL}/N, approximately 83 dB down from the P_g/N curve shown in Fig. 3 which is well below the corresponding P_m/N curve for this case. In the algorithm for the interval attenuation (equation [24]), P_m is needed at two distinct range gates. When the height of the reflection layer, H_j, is near the surface the side-lobe contribution arriving simultaneously with P_m will be larger. For example, if H_j = 0.5 km and D = 1 m then P_{SL}/N is down by about 35 dB from the plotted P_g/N curve in Fig. 3. As compared to $P_m(0.5\ km)/N$ this is an unacceptably high level. To reduce P_{SL} an additional 25 db the antenna diameter would need to be increased to approximately 1.5 m.

The second contribution that arrives at the receiver simultaneous with P_m can be understood by visualizing a ray path incident along the main beam (nadir direction) which scatters out of the vertical direction. This ray is then scattered by the precipitation and received along one of the antenna side lobes. The volume of interest is approximately that portion of the "shell" of two confocal prolate spheroids which contains precipitation. The foci of the ellipsoids are the antenna and the center of the surface illuminated by the main beam (Fig. 4).

To investigate this multi-path contribution to the return power we begin by equating this path length to the mirror reflection path which gives

$$\rho = \left\{ \left(\frac{H_o\ (2H_j + z) + 2H_j^2}{H_o + H_j} \right)^2 - z^2 \right\}^{1/2} : H_s \geq z$$

where ρ is the radial distance measured from the axis of the main antenna beam (vertical) to the multi-path rain volume ΔV. We also define ψ as the angle between the ray directed from the surface to ΔV and the scattered ray from ΔV to the antenna (Fig. 4). Note that for $H_o \gg H_s$, ψ is nearly equal to the bistatic scattering angle θ shown in the figure.

As before H_j is the height of the mirror-reflection layer while z is the height of ΔV which ranges from ground level to the storm top. Table 4 gives values of ρ, ψ and n for three values of H_j; n is the side lobe nearest the main beam into which the scattered energy from ΔV is received (an n = 0 imples that the energy is received along the main beam of the antenna). The results have been tabulated for an altitude of H_0 = 500 km, where we have assumed λ = 1.87 cm, z = H_s = 3 km and parabolic illumination of the reflector.

Table 4

H_0 = 500 km

H_j(km)	ρ(km)	ψ	n		
			D = 1 m	D = 5 m	D = 7.5 m
0.5	2.7	41.8°	0	0	1
1	4	53.3°	0	1	2
3	8.4	71.3°	0	3	6

The large values of ψ in Table 4 indicate that the rain volume of interest is outside the cone into which most of the incident power is bistatically scattered from the surface (see Fig. 5). Moreover, since ψ also represents the bistatic scattering angle of the rain drops, only a fraction of the energy incident on ΔV will be scattered towards the antenna. However, in four of the cases shown in the table, a portion of the multi-path contribution will be received along the main beam of the antenna (n = 0) which produces only a small reduction in the one-way antenna gain. Unfortunately, it is difficult to estimate the magnitude of the multi-path contribution without evaluating the bistastic cross section of the droplets and without accounting for the variations of ψ and ρ throughout the full range of z. Although crude estimates indicate that this contribution is smaller than P_m, more detailed calculations are needed. It should also be noted that a Doppler radar may provide a means of discriminating P_m from side lobe and multi-path contributions (Atlas and Matejka, 1984).

6.2 Bistatic Rain Reflectivity

In the derivation of P_m the bistatic rain reflectivity was replaced by the backscatter reflectivity. The conditions under which the approximation is valid are not as stringent as might be thought since the pairs of surface elements that contribute most to the return power, P_m, are separated by a distance less than the minimum of a_e and $2\rho_o$ (Appendix II). Since a_e is given by $H_j \Gamma \sqrt{8/\sigma^o}$ the range of bistatic scattering angles is given approximately by

$$\pi \geq \psi \geq \pi - \phi$$

where

$$\phi = \mathrm{Tan}^{-1}\left[\min\left(\left(\frac{8\Gamma^2}{\sigma^o}\right)^{1/2}, 2\rho_o/H_j\right)\right]$$

For example, if $\phi = \mathrm{Tan}^{-1}\{(\frac{8\Gamma^2}{\sigma^o})^{1/2}\}$, then for σ^o = 10 dB, and Γ^2 = 0.6 the minimum bistatic scattering angle is approximately 180° − 35° = 145°.

6.3 Mismatches Between Rain Scattering Volumes

Because the ocean surface is roughened by the wind and waves, energy incident on the surface is scattered in all directions. This is why the mirror precipitation echo must be integrated over all scattering angles. The bistatic scatter cross-section corresponding to Eq. (A9) after Ishimaru (1978) is shown in Fig. 5 with windspeed as a parameter. In order to assign a wind speed to each curve, we matched the value of 10 Log σ^o for direct backscatter (i.e., 0 deg) to the corresponding values read from the nadir values of σ^o versus windspeed given by Fedor and Brown (1982) and reproduced in Table 2. Since the latter data were based on observations taken at vertical incidence, while the curves are theoretical, one should not regard them as rigorous. Nevertheless they indicate reasonable behavior. In essence they show that as the wind increases the nadir surface cross-section decreases and that increasing energy is scattered to angles father off nadir. The inset table in Fig. 5 lists the full angle around nadir for which the cumulative power which is scattered from the rain is equal to half the total power radiated back toward the radar. For example, at a windspeed of 10 ms^{-1} (correspond-

ing to 10 Log σ° = 10 dB), we must include the energy scattered from within a cone of 34.4 deg to account for half the total mirror reflected power at the radar.

As indicated in Fig. 5, even light winds will roughen the ocean sufficiently to spread the reflected beams over fairly sizable angles. This has the effect of increasing the horizontal dimensions of the volume of precipitation which is viewed in mirror reflection relative to that which is viewed directly by the incident beam, the more so the higher the volume element. The effects of beam divergence call into question two assumptions made previously. In the derivation of P_m it was assumed that most of the scattering takes place along the vertical, implying that the general path attenuation could be replaced by the attenuation along the vertical. However, as the beam divergence increases, the attenuation must be considered as a weighted average along the various directions of the surface scattered power. The errors resulting from the vertical scattering assumption can be studied quantitatively by including the general path attenuation into the definition of the integral $I(\underline{x}_1, \underline{x}_2)$ (equation (A13)). A study of this type, however, is beyond the scope of this paper. Secondly, in the algorithms for path attenuation, we implicitly assumed that the precipitation within the pulse volume seen in mirror reflection be identical to or of the same reflectivity to that viewed directly. This can be a demanding requirement at a windspeed of 10 ms^{-1}, with the half angle of 17.2 deg, and a pulse volume at 3 km height. The horizontal dimension of the mirror scattering volume is then increased by approximately 0.93 km on either side of the incident beam. For D = 7.5 m, λ = 1.87, H_0 = 500 km the diameter of the incident beam near the surface is approximately 1.2 km. In this case the mirror reflected scattering volume, at a height 3 km above the surface is over a factor of 6 greater than the direct rain scattering volume. On the other hand, for an antenna diameter of 1 m the ratio of the mirror reflected volume to the direct volume decreases to about 1.44.

7. SUMMARY

The method proposed here for the remote measurement of rainfall rate either from space

or aircraft is motivated by the need to circumvent one of the limitations of the single wavelength surface reference technique; namely, that estimates of σ° are required to extract meteorological information from the surface return power. To provide additional information on the surface and meteorological parameters, the mirror-reflected power, P_m, is considered as a possible candidate. P_m corresponds to the portion of the power scattered by the surface, intercepted by the precipitation and returned to the surface where it is scattered a final time back to the antenna. Under a number of simplifications a closed form expression for P_m is obtained. The dependence of P_m on the backscattering cross section, σ°, was found to depend upon the magnitude of the quantity $H_j\ \Gamma/\sqrt{\sigma^\circ}\ \rho_0$, where Γ^2 is the Fresnel reflectivity of the surface, H_j is the height of the reflection layer and ρ_0 is the radius of the FOV. When this quantity is much greater than one, P_m is directly proportional to σ°; if it is much less than one, P_m is independent of σ°. Algorithms based on these limiting cases are proposed for the estimation of path attenuation, rainfall rate and σ°.

The levels of P_m to noise power at nadir over the ocean indicate that detectable signal levels can be obtained from satellite altitudes over a fairly wide rain rate interval. This remains true even with a modest antenna dimension of 1 m. Thus, the method may provide an important auxilliary measurement scheme for a space-borne meterological radar for the estimation of rain and the backscattering cross section of the surface. Estimates of this latter quantity will in turn permit one to investigate the dependence of the mean square surface slope on wind speed in the presence of rain. When the peak transmitted power is reduced from 10 kw to 1 kw, however, the range of detectable rain rates is reduced considerably. Furthermore, over land the decrease in Γ^2 and σ° relative to the ocean background indicates that even at 10 kw, the mirror reflected power as measured from a low earth orbiter will be smaller than the receiver noise power for most rain rates and radar wavelengths.

In the derivation of P_m a number of simplifying assumptions were made both to make the problem tractable and to understand the approximate dependence of P_m on meterological

and surface scattering parameters. Although a qualitative discussion of the error sources is given, quantitative results are needed to check the range of validity of the expressions for P_m and to compare the relative magnitudes of side-lobe and other multi-path contributions that arrive at the antenna simultaneous with P_m.

FIGURE CAPTIONS

Fig. 1: Schematic of the mirror-reflected echo. The mirror-reflection echos which are returned subsequent to the surface return in 1c occur by means of a double reflection from the surface as shown in 1b.

Fig. 2: Curves of the signal to noise ratios for returns from the ocean, P_g, the precipitation viewed directly at a range just above the surfaces P_d, and the mirror-reflected return, P_m, from a 3 km height. Radar parameters are given in Table 1.

Fig. 3: Same as Fig. 2 except for an antenna diameter of 1 m.

Fig. 4: Schematic of a scattering path that arrives at the receiver simultaneous with the mirror-reflected return.

Fig. 5: Bistatic cross section of the ocean for nadir incidence. Inset table shows the conical angle from which 50% of the total power is received.

Fig. A1: Scattering geometry of a ray incident from the radar to the ocean surface element ΔA_1, scattered to the precipitation volume ΔV, and returned to the surface element ΔA_2 where it is scattered a final time back to the radar.

Fig. A2: Schematic of the precipitation volume (ellipsoidal shell) that contributes to the mirror-reflected power for two fixed surface scattering elements.

REFERENCES

Atlas, D., C. W. Ulbrich and R. Meneghini, 1984: The Multi-parameter remote measurement of rainfall. Radio Science, 19, pp. 3-22.

Atlas, D. and T. J. Matejka, 1984: Airborne doppler radar velocity measurements of precipitation seen in ocean surface reflection. Preprints 22nd AMS Conf. on Radar Meterology, Amer. Meteor. Soc., Boston, pp. 548-553.

Atlas, D. and R. Meneghini, 1983: Simultaneous ocean cross-section and rainfall measurements from space with a nadir pointing radar. Preprints 21st Conf. Radar Meteorology, Amer. Meteor. Soc., Boston, pp. 719-726.

Atlas, D., J. Eckerman, R. Meneghini, and R. K. Moore, 1982: The outlook for precipitation measurements from space. Atmosphere-Ocean, 20, pp. 50-61.

Atlas, D. and C. W. Ulbrich, 1977: Path-and area integrated rainfall measurements by microwave attenuation in the 1-3 cm band. J. Appl. Meteor. 16. pp. 1322-1331.

Atlas, D. and O. Thiele (eds.), 1981. Precipitation measurements from space. Workshop Report NASA/Goddard Space Flight Center. 431 pp.

Battan, L. J., 1973: Radar Observation of the Atmosphere. University of Chicago Press, Chicago, 324 pp.

Eccles, P. J. and E. A. Mueller, 1971: X-band attenuation and liquid water content estimation by a dual-wavelength radar. J. Appl. Meteor., 10, pp. 1252-1259.

Eckerman, J., R. Meneghini and D. Atlas, Average Rainfall determination from a scanning beam spaceborne meteorological radar. NASA Tech. Memo. 79664, Nov., 1978.

Fedor, L. S. and G. S. Brown, 1982: Wave height and windspeed measurements from the SEASAT radar altimeter. J. Geophysical Research, 87, pp. 3254-3260.

Fujita, M., 1983: An algorithm for estimating rain rate by a dual-frequency radar. Radio Science, 18, 697-708.

Fujita, M., K. Okamoto, S. Yoshikado and K. Nakamura, 1984: Inference of rain rate profile and path-integrated rain rate by an airborne microwave rain scatterometer/radiometer. Preprints 22nd AMS Conference on Radar Meterology, Amer. Metero. Soc., Boston, pp.

Gradshteyn, I. S. and I. M. Ryzhik, 1965 Tables of Integral, Series and Products. Fourth ed., p. 178, 1086 pp.

Hitschfeld, W. and J. Bordan, 1954: Errors inherent in the radar measurement of rainfall at attenuating wavelengths. J. Meteor., 11, pp. 58-67.

Inomata, H., et al., 1981: Remote sensing of rainfall rates using airborne microwave rain-scatterometer/radiometer. Proc. 15th Int. Symp. on Remote Sensing of Environment, Ann Arbor, Mich.

Ishimaru, A., 1978: Wave Propagation and Scattering in Random Media, Vol. 2. Academic Press, New York, 572 pp.

Lu, Da-ren, and Lin Hai, 1980: Comparisons of radar and microwave radiometer in precipitation measurements and their combined use. Acta Atmospherica Sinic, 1980: No. 1. (in Chinese).

Meneghini, R., J. Eckerman and D. Atlas, 1983: Determination of rain rate from a spaceborne radar using measuring of total attenuation. IEEE Trans. GeoScience and Remote Sensing, GE-21, pp. 34-43.

Morse, P. M. and H. Feshbach, 1953: Methods of Theoretical Physics, Vol. 1, § 5.1, McGraw-Hill, New York, 997 pp.

Moore, R. K., and A. K. Fung, 1979: Radar determination of winds at sea, pro. IEEE, 67, pp. 1504-1521.

Probert-Jones, J. R., 1962: The radar equation in meterology. Quart. J. Roy. Meteor. Soc., 88, pp. 485-495.

Silver, S., 1949: Microwave Antenna Theory and Design, § 6.8, MIT Radiation Laboratory Series, McGraw-Hill, New York, 623 pp.

Wilheit, T. T. et al., 1977: A satellite technique for quantitatively mapping rainfall rates over the oceans. J. Appl. Meteor., 16, pp. 551-560.

APPENDIX I

Table of Symbols

λ	–	Wavelength
P_T	–	Peak transmitted power
P_t	–	Transmitted power waveform
t	–	Transmitted pulse duration
$L/2$	–	Range resolution
H_0	–	Orbit altitude
H_j	–	Height of rain layer
H_s	–	Height of storm
σ^*	–	Ocean cross-section at nadir
$\sigma_b(\hat{i}, \hat{o})$	–	Ocean normalized bistatic cross-section; incident wave in the $\hat{i}$ direction, scattered wave in the direction $\hat{o}$.
θ_b	–	3 db beamwidth measured from the peak to the half power point.
A_e	–	Effective antenna area
G_0	–	Antenna gain along beam axis
$G_t(\hat{i})$	–	Antenna gain pattern along the ith direction on transmit
$G_r(\hat{i})$	–	Antenna gain pattern along the ith direction on receive
$\eta(\hat{i}, \hat{o})$	–	Bistatic rain reflectivity
η	–	Backscattered rain reflectivity
R	–	Path-averaged rain rate
k	–	Attenuation coefficient
Z	–	Rain reflectivity factor
A	–	Path-integrated attenuation
P_m	–	Mirror reflected echo power

Table of Symbols

P_d	–	Echo power directly scattered from precipitation.
P_g	–	Echo power directly scattered from ocean surface.
N	–	Receiver noise power
c	–	Speed of light in free space

APPENDIX II

The purpose of the appendix is to derive approximate expressions for the return power P_m. P_m corresponds to the portion of the power scattered by the surface which is intercepted by the precipitation, returned again to the surface and is scattered back to the antenna. A general ray path contributing to P_m is shown in Fig. A1 and can be written as

$$\Delta P_m(t) = \frac{P_t\ (t - \sum_0^3 r_i/c)}{(4\pi)^4\ (r_0\ r_1\ r_2\ r_3)^2}\ G_t(\hat{r}_0)$$

$$* (\sigma_b(\hat{r}_0; \hat{r}_1)\ \Delta A_1) * (\eta(\hat{r}_1; \hat{r}_2)\ \Delta V)$$

$$* (\sigma_b(\hat{r}_2; \hat{r}_3)\ \Delta A_2) * A_e\ \ 10^{-0.1 \int_Q k\ ds} \qquad (A1)$$

where Q is that portion of the ray path within the precipitation and where the symbols in (A1) are defined in Appendix I.

Assuming that ΔA_1, ΔA_2, and ΔV can be converted into differential area and volume elements, and using the relation $A_e = \lambda^2\ G_r/4\pi$ then P_m can be written

$$P_m(t) = \frac{\lambda^2}{(4\pi)^5} \int_{\underline{x}_1} \int_{\underline{x}_2} \frac{G_t(\hat{r}_0)\ G_r(\hat{r}_3)}{r_0^2\ r_3^2}\ d\underline{x}_1\ d\underline{x}_2$$

$$\times \left\{ \int_V P_t(t - \sum_0^3 r_i/c)\ \frac{\sigma_b(\hat{r}_0; \hat{r}_1)\ \sigma_b(\hat{r}_2; \hat{r}_3)\ \eta(\hat{r}_1; \hat{r}_2)}{r_1^2\ r_2^2}\ 10^{-0.1 \int_Q k\ ds}\ dV \right\} \qquad (A2)$$

where the volume integral is taken over the precipitation, and $d\underline{x}_1$, $d\underline{x}_2$ are elements of surface area. The range of integration on both $\underline{x}_1$, $\underline{x}_2$ is the portion of the surface illuminated by the main beam. Let the transmitted pulse be rectangular and of duration τ with P_T the peak transmitted power

$$P_t\ (t) = P_T\ [U(t) - U(t - \tau)] \qquad (A3)$$

where U is the unit step function. Therefore,

$$P_t(t - \sum_0^3 r_i/c) = P_T\,[U(t - T - (r_1 + r_2)/c) - U(t - T - (r_1 + r_2)/c - \tau)] \qquad (A4)$$

If $H_o >> \rho_o$ where H_o is the spacecraft altitude and ρ_o is the radius of the footprint, then

$$T \approx 2H_o/c + (|x_1|^2 + |x_2|^2)/2H_o\, c \qquad (A5)$$

where $|\underline{x}_1|$, $|\underline{x}_2|$ are the distances measured from the center of the footprint to $\underline{x}_1$, $\underline{x}_2$, respectively. Thus P_t is non zero for

$$2H \leq r_1 + r_2 < 2(H + L/2) \qquad (A6)$$

where $L/2$ is the range resolution, equal to $c\tau/2$, and

$$2H = ct - 2H_o - (|x_1|^2 + |x_2|^2)/2H_o - c\tau \qquad (A7)$$

The condition given by (A6) specifies the region of precipitation that contributes to P_m. In particular, for a fixed observation time and fixed $\underline{x}_1$; $\underline{x}_2$ the volume integral taken over the precipitation is that region contained within a prolate spheroidal 'shell' with foci at $\underline{x}_1$, $\underline{x}_2$ (Fig. A2).

Using a coordinate system whose origin is mid-way between $\underline{x}_1$, $\underline{x}_2$ and whose x-axis passes through both points, the family of prolate spheroids within this region can be expressed by the equation (Morse and Feshbach, 1953)

$$\frac{x^2}{\zeta^2 - \alpha^2} + \frac{(y^2 + z^2)}{\zeta^2 - \beta^2} = 1;\ \zeta > \beta \geq \alpha \qquad (A8)$$

where $\zeta_{min} \leq \zeta \leq \zeta_{max}$ with

$$\begin{aligned} \zeta_{min} &= (H^2 + \alpha^2)^{1/2} \\ \zeta_{max} &= [(H + L/2)^2 + \alpha^2]^{1/2} \end{aligned} \qquad (A9)$$

The distances between the points $\underline{x}_1$ and $\underline{x}_2$ is given by $2x_0$ where

$$x_0 = (\beta^2 - \alpha^2)^{1/2}$$

To simplify the expression for P_m, we make the following approximations

(a) The bistatic rain reflectivity factor, $\eta(\hat{r}_1; \hat{r}_2)$, can be replaced by the backscattered rain reflectivity, η.

(b) The majority of the power backscattered from the surface is directed along the vertical direction so that the attenuation can be approximated by the attenuation along the vertical direction, i.e.

$$\int_Q k\, ds \approx 2 \int_0^{H_s} k\, dz + 2 \int_0^{H} k\, dz$$

where H_s is the storm height. We assume, moreover that H can be interpreted as the height of the reflection layer and that H is nearly independent of $\underline{x}_1$, $\underline{x}_2$.

(c) The spacecraft or aircraft altitude is taken to be much greater than the radius of the main-beam footprint: $H_o >> \rho_o$. This implies that the 'ray' paths $\underline{r}_0$, $\underline{r}_3$ shown in Fig. (A1) are nearly vertical so that

$$\sigma_b(\hat{r}_0; \hat{r}_1) \approx \sigma_b(-\hat{z}; \hat{r}_1) = f(\theta_1)$$

$$\sigma_b(\hat{r}_2; \hat{r}_3) \approx \sigma_b(\hat{r}_2; \hat{z}) = f(\theta_2)$$

where the angles θ_1, θ_2 are defined in Fig. (A2).

(d) The bistatic cross section of the surface for incident energy along the vertical which is scattered at an angle θ is given by the scalar Kirchhoff approximation for a very rough surface (Ishimaru: 1978):

$$f(\theta) = \frac{2m\Gamma^2}{(1 + \cos\theta)^2}\, e^{-\frac{m}{2}\tan^2\theta/2} \qquad (A10)$$

where Γ^2 is the Fresnel reflectivity of the surface and $m = \ell^2/2\beta_o^2$ where ℓ is the correlation length of the surface and β_o is the rms surface height.

(e) Assuming a Gaussian antenna pattern, the antenna gains are written

$$G_t(\hat{r}_0) = G_o\, e^{-(\gamma\theta_1/\theta_b)^2} \approx G_o\, e^{-\beta^2\rho_1^2}$$

$$G_r(\hat{r}_3) = G_o\, e^{-(\gamma\theta_2/\theta_b)^2} \approx G_o\, e^{-\beta^2\rho_2^2}$$

where θ_b is the beamwidth measured from the maximum to the half power point and where

$$G_o = \pi^2/(2\theta_b)^2$$

$$\gamma = 0.831$$

$$\beta = \gamma/\theta_b H_o \approx \gamma/\rho_o$$

The quantities ρ_1, ρ_2 are the respective distances from the center of the field of view (FOV) to the scattering centers $\underline{x}_1$, $\underline{x}_2$ on the surface (i.e. $\rho_1 = |\underline{x}_1|$, $\rho_2 = |\underline{x}_2|$) while ρ_o is the radius of the FOV.

The validity of these approximations is discussed in the text. With these assumptions (A2) can be written

$$P_m(t) = \frac{\lambda^2\, G_o^2\, P_T\, \eta}{(4\pi)^5\, H_o^4}\; 10^{-0.2(A_n + A)}\; J \qquad \text{(A11)}$$

where

$$J = \int_{\underline{x}_1}\int_{\underline{x}_2} e^{-\beta^2(\rho_1^2 + \rho_2^2)}\; I(\underline{x}_1, \underline{x}_2)\; d\underline{x}_1\, d\underline{x}_2 \qquad \text{(A12)}$$

$$I(\underline{x}_1, \underline{x}_2) = \int_V \frac{f(\theta_1)\, f(\theta_2)}{r_1^2\, r_2^2}\, dV \qquad \text{(A13)}$$

$$A_n = \int_0^{H_s} k\, dz; \quad A = \int_0^{H} k\, dz \qquad \text{(A14)}$$

where the observation time t corresponds to the reflection layer height, H and where $f(\theta)$ is given by (A10).

To express the volume integration of (A13) as an iterated integral, we first note from Fig. A2 that $\cos \theta_2 = z/r_2$, $\cos \theta_1 = z/r_1$ and therefore $\cos \theta_2 = r_1 \cos \theta_1 / r_2$.

For any point (x, y, z) within the spheroidal 'shell' shown in Fig. A2 we have

$$r_1 = [(x + x_0)^2 + y^2 + z^2]^{1/2}$$

$$r_2 = [(x - x_0)^2 + y^2 + z^2]^{1/2}$$

where as before the origin of the coordinate system is taken midway between the two scattering centers where the x-axis passes through $\underline{x}_1$ and $\underline{x}_2$. Therefore,

$$r_1 = (r_2^2 + 4xx_0)^{1/2} \tag{A15}$$

Choosing a spherical coordinate system with an origin at $x = x_0$, an arbitrary point (x, y, z) in the reference system can be expressed by

$$\begin{aligned} x &= x_0 + r_2 \sin \theta_2 \cos \phi_2 \\ y &= r_2 \sin \theta_2 \sin \phi_2 \\ z &= r_2 \cos \theta_2 \end{aligned} \tag{A16}$$

Substituting (A16) into (A15) gives

$$r_1 = r_2 F \tag{A17}$$

where

$$F = \left[1 + \frac{4x_0}{r_2} \sin \theta_2 \cos \phi_2 + \frac{4x_0^2}{r_2^2} \right]^{1/2} \tag{A18}$$

so that

$$\cos \theta_1 = \cos \theta_2 / F \tag{A19}$$

Using (A19) and (A10) the function $f(\theta_1)$ can be written in terms of r_2, ϕ_2, θ_2. Explicitly, $f(\theta_1) = \tilde{f}(r_2, \phi_2, \theta_2)$ where

$$\tilde{f}(r_2, \phi_2, \theta_2) = \frac{2m\ \Gamma^2}{(1 + \cos\theta_2/F)^2} \exp\left[-\frac{m}{2} (1 - \cos^2\theta_2/F)/(1 - \cos\theta_2/F)^2 \right] \quad (A20)$$

Therefore (A13) becomes

$$I(\underline{x}_1, \underline{x}_2) = \int_{\theta=0}^{\pi/2} \int_{\phi=0}^{2\pi} \int_{r=r_A}^{r_B} \frac{f(\theta)\ \tilde{f}(r, \phi, \theta)}{r^2\ F^2} \sin\theta\ dr\ d\phi\ d\theta \quad (A21)$$

The limits on r can be found by substituting equations (A10) into (A8) and solving r_2 when $\zeta = \zeta_{min}, \zeta_{max}$. This procedure gives

$$r_A(\phi, \theta) = (H^2 - x_0^2)/(H + x_0 \sin\theta \cos\phi)$$

$$r_B(\phi, \theta) = [(H + L/2)^2 - x_0^2]/[(H + L/2) + x_0 \sin\theta \cos\phi] \quad (A22)$$

In spite of the simplifications made, the integral (A12) with I given by (A21) is formidable. To further simplify (A21) we use the fact that a good approximation to $I(\underline{x}_1, \underline{x}_2)$ is

$$I(\underline{x}_1, \underline{x}_2) = I_s\ e^{-\alpha^2 |x_1 - x_2|^2} \quad (A23)$$

where

$$I_s = \frac{\pi\ L\ \Gamma^2}{H}\ \sigma^\circ \quad (A24)$$

$$\alpha^2 = 1/a_e^2 = \sigma^\circ/8\ \Gamma^2\ H^2 \quad (A25)$$

and where σ° is the normalized backscattering cross section of the surface for nadir incidence.

To understand qualitatively why $I(\underline{x}_1, \underline{x}_2)$ can be approximated by this function we first note that as $\underline{x}_2 \to \underline{x}_1$, (A21) becomes

$$I(\underline{x}_1, \underline{x}_1) \equiv I_s = 2\pi \int_{\theta=0}^{\pi/2} \int_{r=H}^{H+L/2} \frac{f^2(\theta)}{r^2} \sin\theta\ dr\ d\theta \quad (A26)$$

Making the change of variable $u = \tan^2(\theta/2)$ and using (A10), (A26) can be integrated to give

$$I_s = 2\pi(H^{-1} - (H + L/2)^{-1}) \frac{(\Gamma^2 m)^2}{2} \left\{ \frac{1 - 4e^{-m}}{m} + \frac{2(1 - 2e^{-m})}{m^2} + \frac{2(1 - e^{-m})}{m^3} \right\} \tag{A27}$$

From Ishamaru (1978), we have

$$m = 2\sigma^\circ/\Gamma^2$$

Since for most sea states $m >> 1$, we can neglect terms of order m^{-2}, m^{-3}, and e^{-m}. Furthermore, assuming that $H >> L/2$ then I_s reduces to (A24).

The second feature of $I(\underline{x}_1, \underline{x}_2)$, i.e., its dependence on $|\underline{x}_1 - \underline{x}_2|$ and a_e can be understood by noting that the integrand of $I(\underline{x}_1, \underline{x}_2)$ is proportional to $f(\theta_1)\, f(\theta_2)$ where

$$f(\theta_1)\, f(\theta_2) \propto \exp\left[- \frac{m}{2} (\tan^2 (\theta_1/2) + \tan^2 (\theta_2/2)) \right]$$

Letting $\theta_1 = \theta_2 = \theta$ we obtain $f^2(\theta) \propto e^{-1}$ when $\tan\theta = 2\sqrt{m}/(m - 1)$. The angle θ can be related to the distance between the scattering centers, a_e, by noting that

$$a_e = 2H \tan\theta$$

or, using the above result for $\tan\theta$ and $m = 2\sigma^\circ/\Gamma^2 >> 1$, then

$$a_e = 4H\Gamma / \sqrt{2\sigma^\circ}$$

Returning to (A23) and substituting this equation into (A12) and expressing $\underline{x}_1$, $\underline{x}_2$ in cylindrical coordinates we obtain

$$J = I_s \int_{\rho_1=0}^{\infty} \int_{\rho_2=0}^{\infty} e^{-(\alpha^2 + \beta^2)(\rho_1^2 + \rho_2^2)} \rho_1 \rho_2 \left\{ \int_{\phi_1=-\pi}^{\pi} \int_{\phi_2=-\pi}^{\pi} e^{2\alpha^2 \rho_1 \rho_2 \cos(\phi_1 - \phi_2)} d\phi_1\, d\phi_2 \right\} d\rho_1\, d\rho_2 \tag{A28}$$

To perform the integrals over ϕ_1, ϕ_2 we make the transformation

$$u = \phi_1 - \phi_2$$

$$v = \phi_2$$

The double integral over ϕ_1, ϕ_2 then becomes

$$I_1 = \int_{v=-\pi}^{\pi} \int_{u=-\pi-v}^{\pi-v} e^{2\alpha^2 \rho_1 \rho_2 \cos u} \, du \, dv$$

but,

$$\int_{u=-v-\pi}^{\pi-v} e^{p \cos u} \, du = 2 \int_{0}^{\pi} e^{p \cos u} \, du = 2\pi I_0(p)$$

where I_0 is the modified Bessel function of the first kind, zeroth order.

Therefore,

$$I_1 = 4\pi^2 I_0(2\alpha^2 \rho_1 \rho_2) \tag{A29}$$

Substituting (A29) into (A28) gives

$$J = 4\pi^2 I_s \int_{\rho_2=0}^{\infty} \int_{\rho_1=0}^{\infty} I_0(2\alpha^2 \rho_1 \rho_2) \, e^{-(\alpha^2 + \beta^2)(\rho_1^2 + \rho_2^2)} \rho_1 \rho_2 \, d\rho_1 d\rho_2 \tag{A30}$$

Carrying out the remaining integrations (Gradshteyn and Ryzhik, 1965) yields

$$J = \frac{\pi^2 I_s}{\beta^2 [2\alpha^2 + \beta^2]} \tag{A31}$$

Substituting (A31) into (A11) and using the definitions of α, β and G_0 gives equation (6) of the text.

To calculate the ground return we assume that beam-limited conditions hold and we choose, as before, a Gaussian antenna gain. We obtain

$$P_g = \frac{P_T G_0^2 \sigma^\circ \lambda^2}{2^7 \pi^2 \beta^2 H_0^4} \, 10^{-0.2 A_n}$$

Using $G_o = \pi^2/4\theta_b{}^2$ and the definition of β, yields equation (2) of the text. The expression for the direct rain return, equation (3) is essentially equivalent to that derived by Probert-Jones (1962) for a rotationally symmetric antenna pattern.

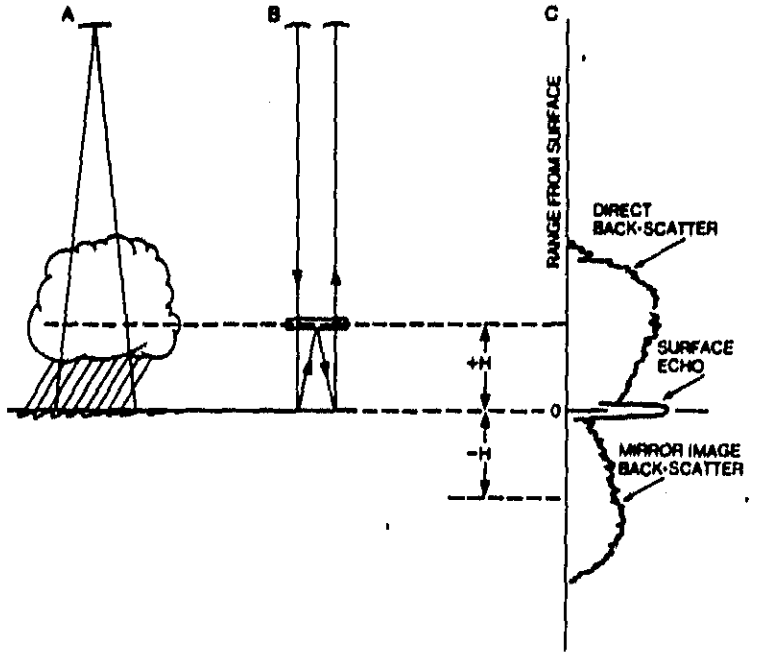

Figure 1. Schematic of the mirror-reflected echo. The mirror-reflected echos which are returned subsequent to the surface return in 1c occur by means of a double reflection from the surface as shown in 1b.

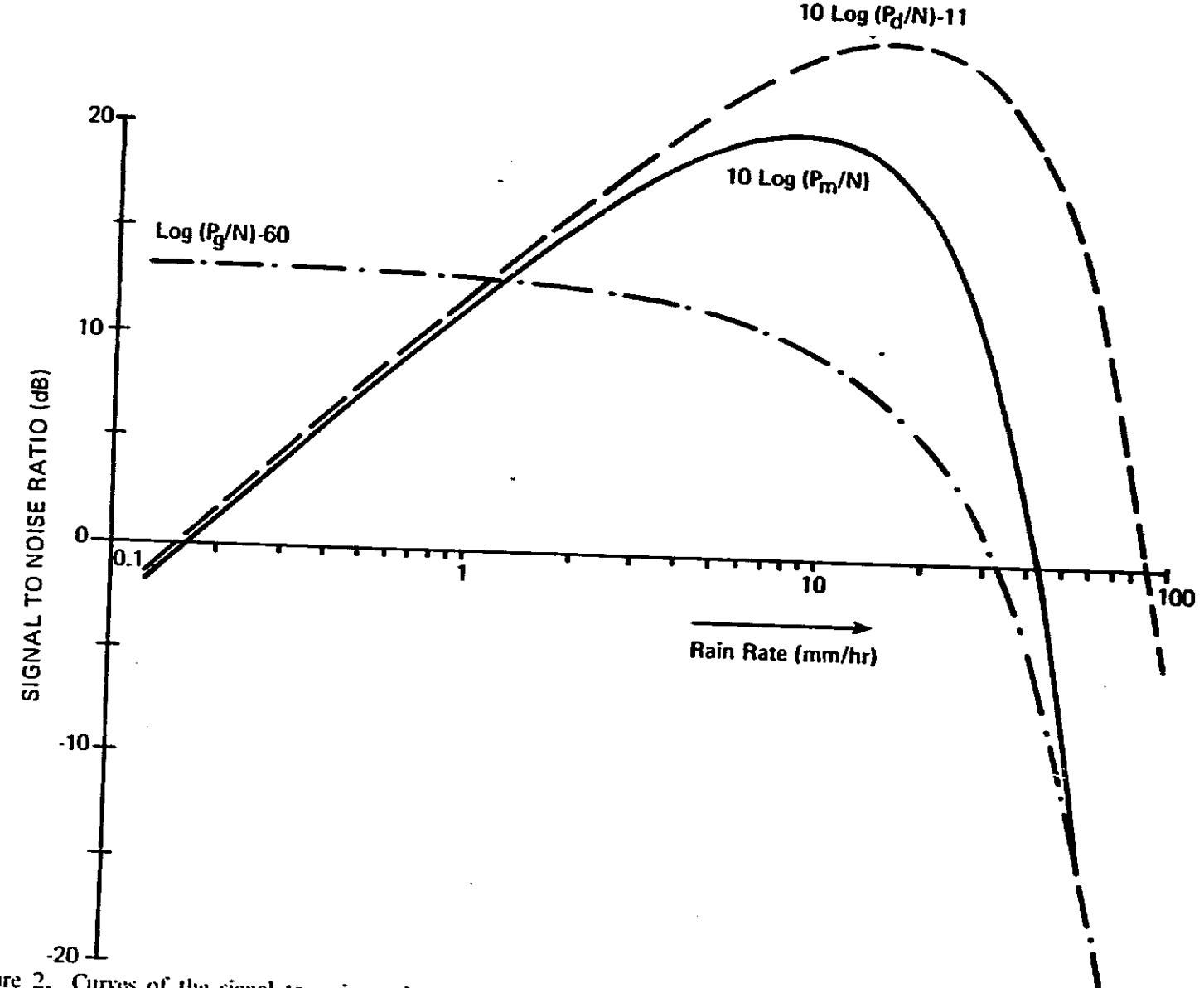

Figure 2. Curves of the signal to noise ratios for returns from the ocean P_g, the precipitation viewed directly at a range just above the surface P_d, and the mirror-reflected return, P_m, from a 3 km hieght. Radar parameters are given in Table 1.

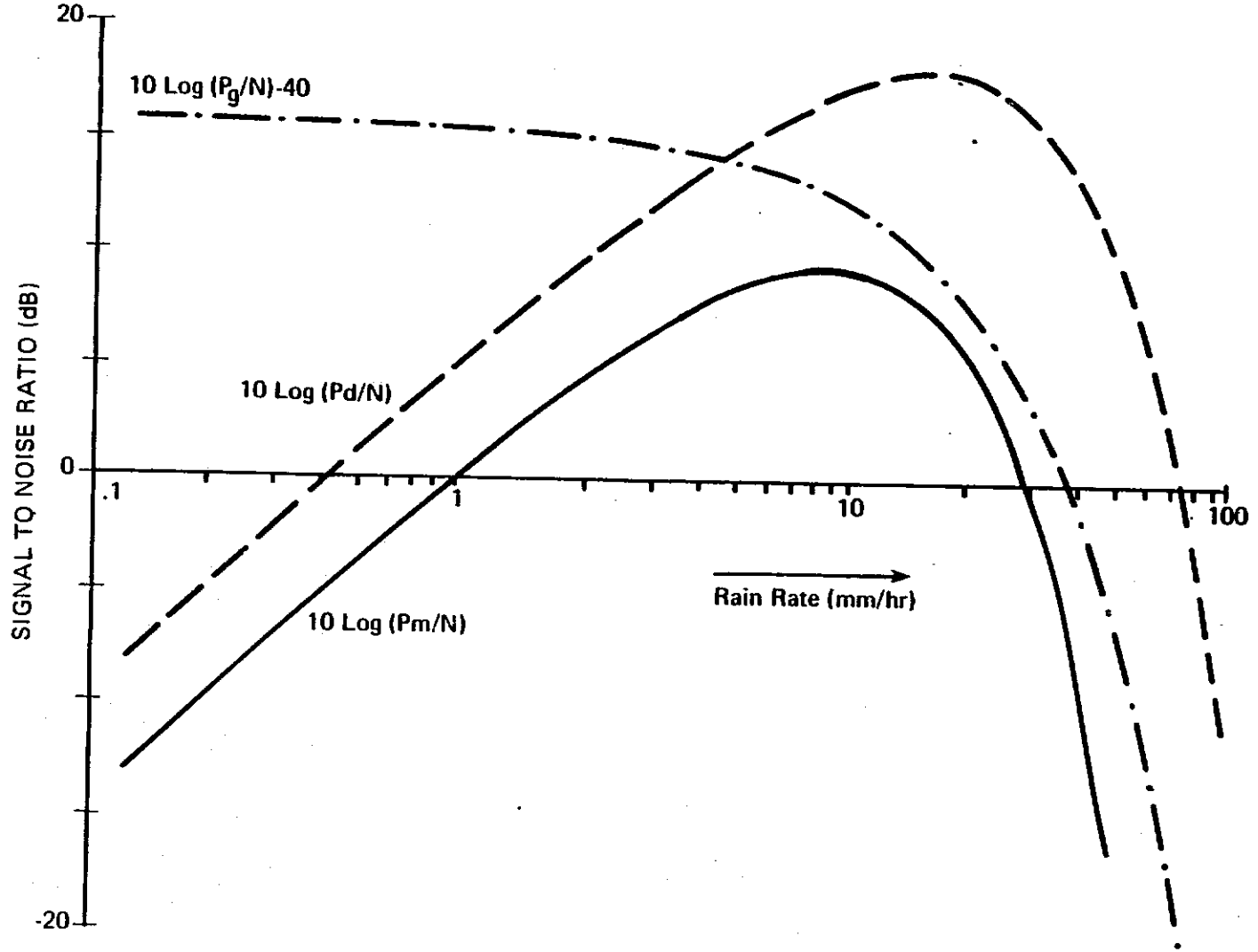

Figure 3. Same as Fig. 2 except for an antenna diameter of 1 m.

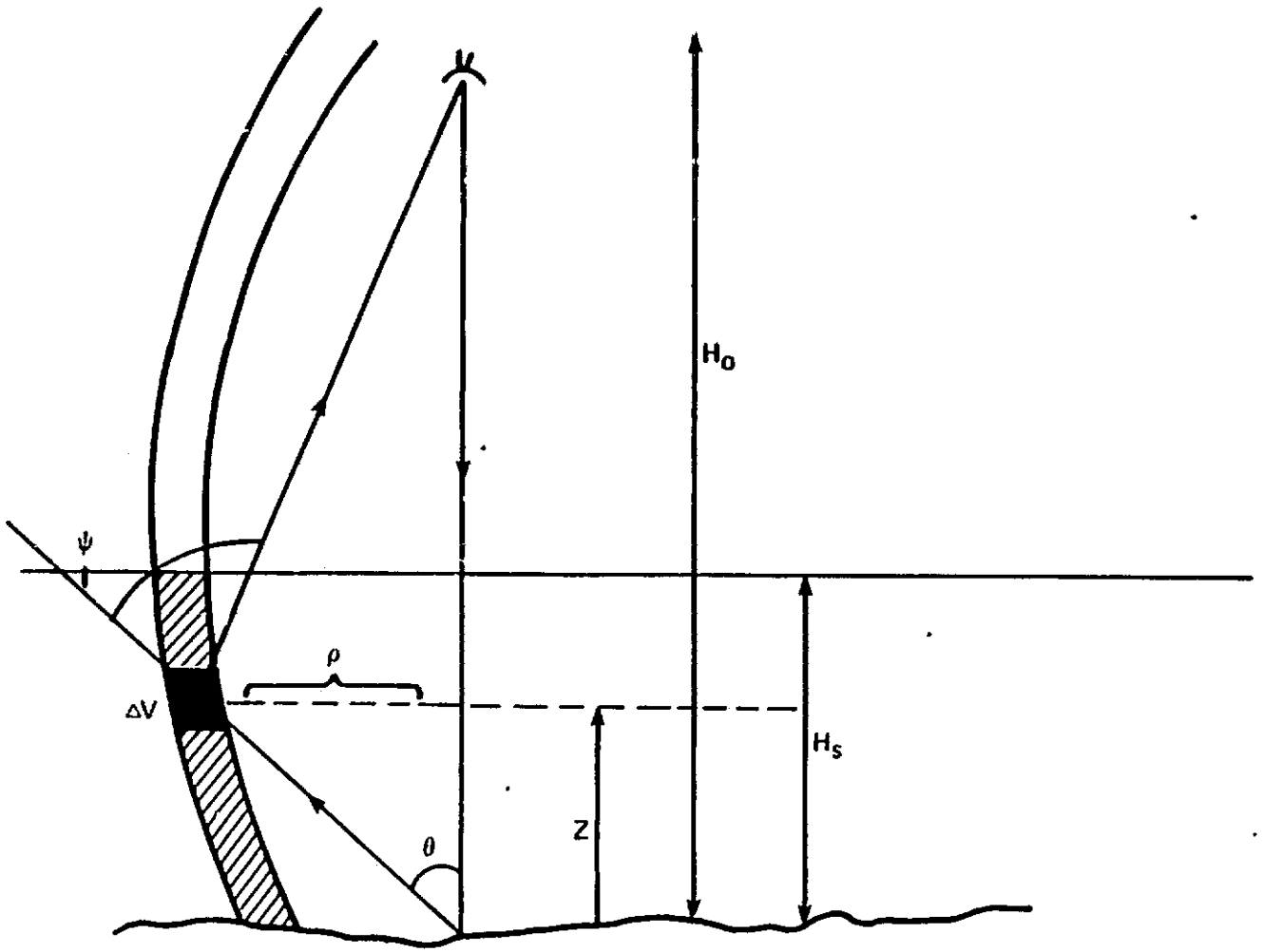

Figure 4. Schematic of a scattering path that arrives at the receiver simultaneous with the mirror-reflected return.

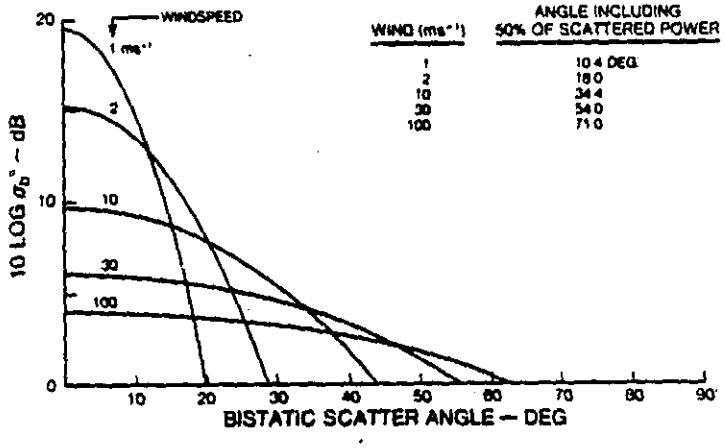

Figure 5. Bistatic cross section of the ocean for nadir incidence. Inset table shows the conical angle from which 50% of the total power is received.

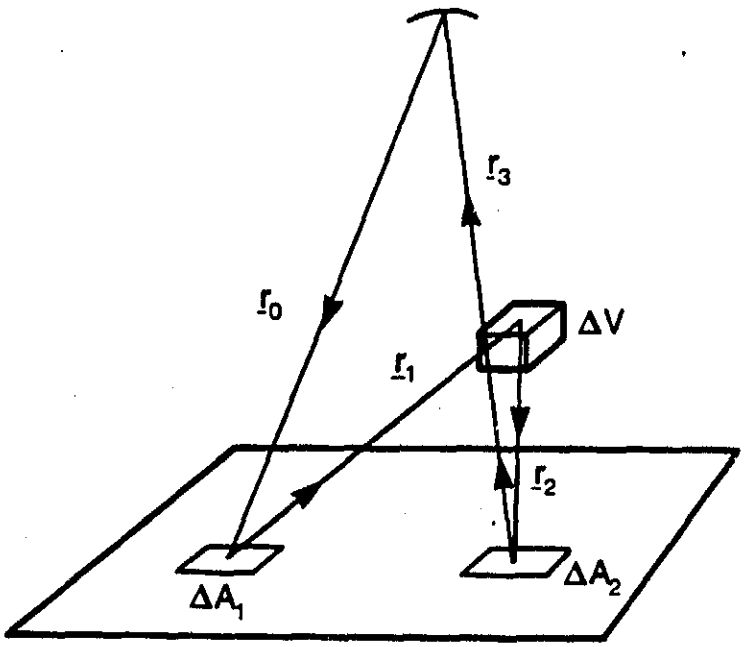

Figure A1. Scattering geometry of a ray incident from the radar to the ocean surface element ΔA_1, scattered to the precipitation volume ΔV, and returned to the surface element ΔA_2 where it is scattered a final time back to the radar.

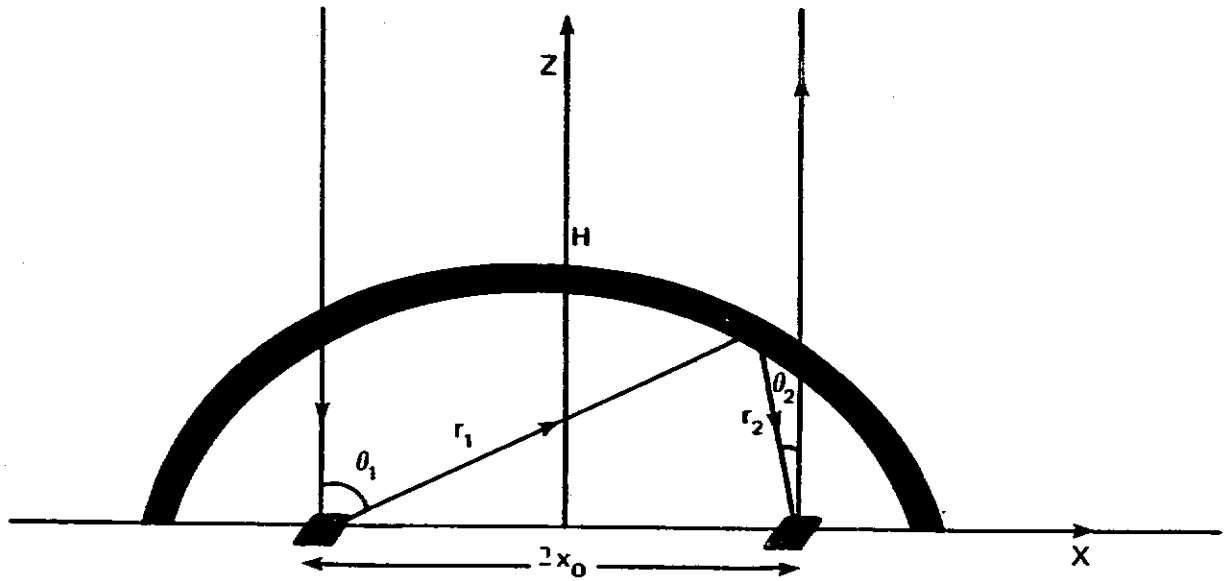

Figure A2. Schematic of the precipitation volume (ellipsoidal shell) that contributes to the mirror-reflected power for the two fixed surface scattering elements.